Contact Characteristics of a Laser Scanner Motor in a Laser Printer in the Low Speed Region*

Hiroyuki Kawamoto✦

Department of Mechanical Engineering, Waseda University, Tokyo, Japan

This article describes a transient contact phenomenon during start-stop operation of a polygonal mirror scanner rotor driven by a flat-type brushless DC motor and supported by a passive thrust magnetic bearing and a radial air bearing. From experimental investigations, the following characteristics have been clarified. The rotor is statically unstable in the very low speed region. This instability occurs because the stiffness of the air bearing is not induced without rotation, and it is small in the very low speed region, whereas the magnetic negative stiffness of the magnetic bearing exists even at zero speed. Dry contact between the rotor and the stator is induced at the speed lower than a threshold, because a static displacement due to the gravity and non-uniform magnetization of the magnetic bearing and forced vibration due to unbalance of the rotor exceed the air gap of the air bearing. Vertical support of the rotor results in the increase of the threshold speed, in the order of several tens percent, compared to horizontal support. Vibration due to unbalance of the rotor scarcely affects the contact phenomenon. Because dry contact reduces the lifetime of the air bearing, it is preferable to avoid frequent start–stop operations and to keep the rotor speed higher than the threshold. The instability is reduced by adopting a magnetic bearing composed of a pair of permanent magnets.

Journal of Imaging Science and Technology 45: 489—494 (2001)

Introduction

A polygonal mirror scanner motor is used in the exposure subsystem of digital electrophotography to scan the laser beam and thereby write latent images on the photoreceptor.[1,2] The rotation of the mirror is required to have (1) stablity, constant velocity, and low vibration, to realize high image quality; (2) high speed rotation for high print speed and high resolution machines; (3) long life; (4) small power loss; (5) low acoustic noise; and (6) low cost. The motor shown in Fig. 1 and Fig. 2 is under development to meet these requirements. The rotor is driven by a flat-type brushless and coreless DC motor. The polygonal mirror is attached to the rotor. The rotor is supported in the radial direction by an outer-rotor-type self-acting grooved journal air bearing[3–8] and in the axial direction by an axially stable passive magnetic bearing.[9,10] The magnetic bearing utilizes an axial restoring magnetic force between radially magnetized rotor and stator magnets made of plastic magnetic material.

Two types of excessive transient vibration take place in this rotor system during the startup and free-run operations. One is an axial displacement and vibration during start–stop operation and another is radial dry-contact in the very low speed region. The former is caused by the axial magnetic repulsive force induced in the flat motor. It prolongs the startup time and, in the worst case, the rotor collides with a casing in the axial direction. The mechanism of this vibration has been clarified and some countermeasures have been proposed.[11] On the other hand, the latter is due to the decrease of effective radial stiffness in the very low speed region. This occurs because the stiffness of the self-acting air bearing is not induced without rotation and it is small in the very low speed region, whereas the magnetic negative stiffness of the magnetic bearing exists in the radial direction even at zero speed. Dry contact between the rotor and shaft is induced at a speed lower than a threshold. It causes wear of the air bearing or abrasion fragments that are accidentally caught in the bearing gap. These reduce the lifetime of the scanner motor.

Although the motor had been designed to be supported horizontally to avoid the radial displacement and anisotropic effect due to the gravity, vertical or oblique support is required for a new desktop color printer to set the scanner system in a restricted small area. Hence, the dry-contact phenomenon must be clarified strictly in order to utilize this type of scanner for desktop machines. The objectives of the present investigation are to clarify qualitative characteristics of the dry-contact, to evaluate the effect of gravity, and to propose an evaluation method and effective countermeasures in order to realize highly reliable and compact digital copy machines and laser printers.

Experimental

Experimental Procedure

Figure 3 shows an experimental setup to measure the change of torque during start and stop operations. The

Original manuscript received June 5, 2000

✦ IS&T Fellow; kawa@mn.waseda.ac.jp

* A portion of this article has been presented at the Image Processing Image Quality Image Capture Systems Conference (PICS2000) at Portland, Oregon in March 27, 2000.

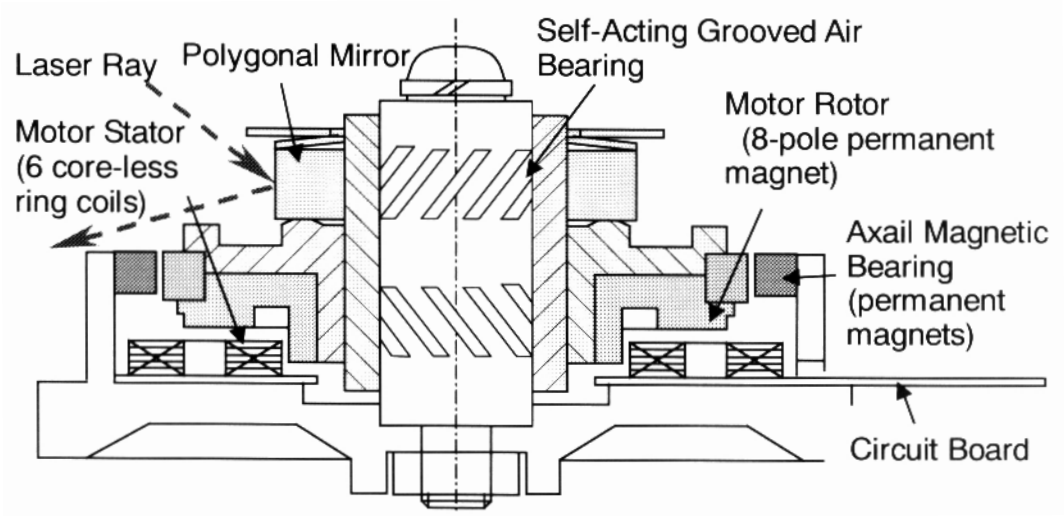

Figure 1. Configuration of polygonal mirror scanner rotor driven by flat-type brushless DC motor and supported by axial magnetic and radial air bearing.

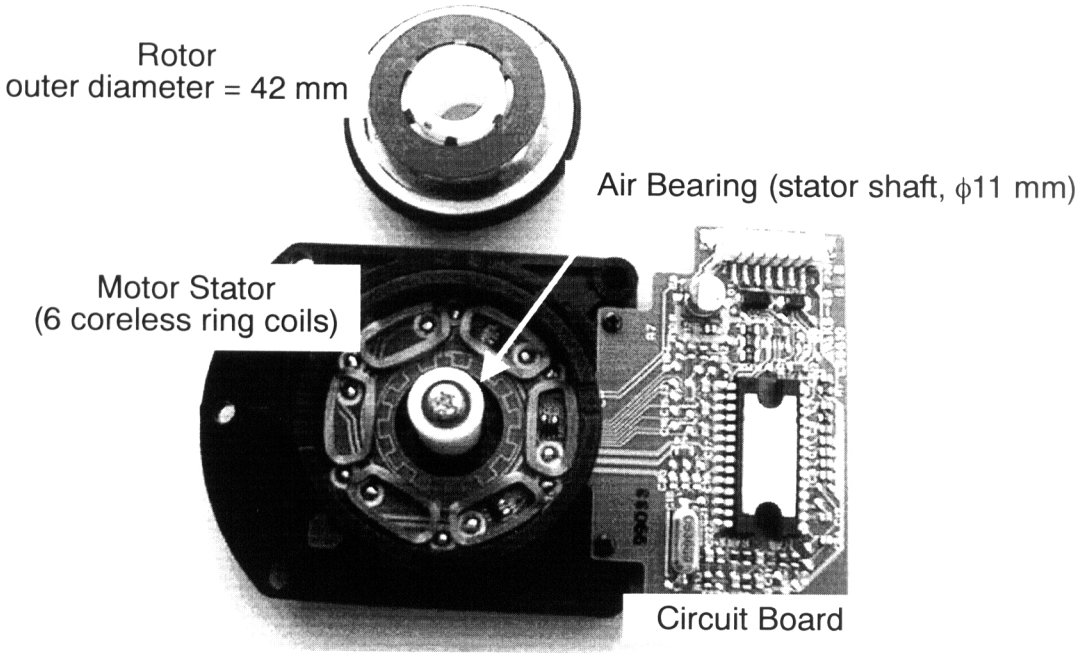

Figure 2. Polygonal mirror scanner motor. The rotor (upper) is disassembled from the stator (lower).

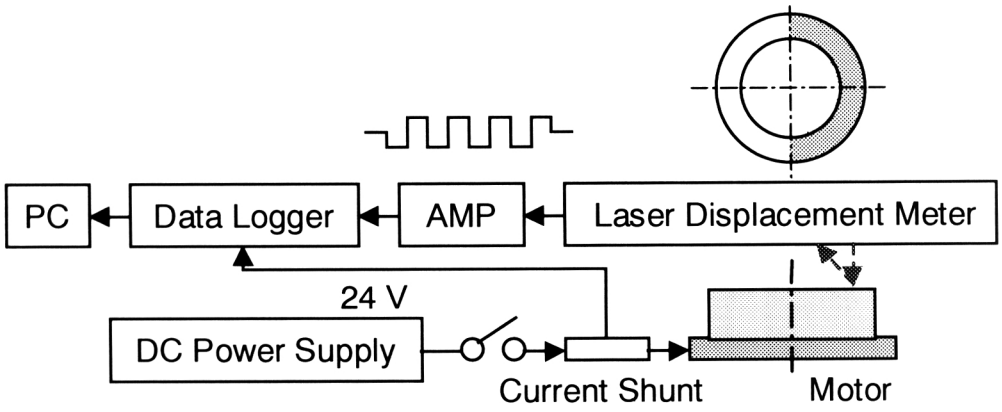

Figure 3. Experimental setup.

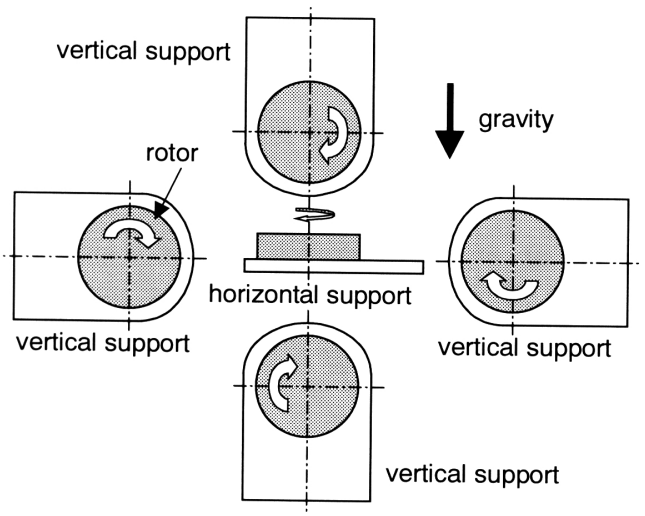

Figure 4. Vertical and horizontal support of rotor.

motor consists of a ring-shape rotor made of an 8-pole permanent magnet and six coreless stator coils. The stator coils, which consist of three pairs of U, V, and W-phase coils, are star-connected. The rated speed of the motor is 20,400 rpm. A black-and-white mark is painted on the top of the rotor and a pulse wave of laser beam reflection was measured by a laser displacement meter (Keyence Corp., Osaka, Japan, LK-2000). The signals were digitized and sent to a computer where data were numerically transformed to the speed.

Experiments were performed under condition of horizontal and vertical support as shown in Fig. 4. Three motors were used to examine individual difference. The effect of mechanical unbalance of the rotor was investigated using one of the motors. All of the measurements were conducted three times under the same condition to confirm reproducibility.

Free Vibration

Figure 5 shows an example of axial free vibration at zero speed. It is well known that the free vibration shows an exponential decay form with viscous damping, but it is arithmetical with dry friction. Because the rotor was in contact with the stator, the free vibration decay was not exponential but arithmetical. The measured frequency of the vibration was 43.7 Hz, which corresponded to the 2.9 N/mm axial stiffness of the magnetic bearing. This dynamically derived stiffness coincided with the statically measured value derived by dividing weights put on the rotor by the static displacement measured by the laser displacement meter. The frictional force was 0.021 N, which was derived from the arithmetical decay.

Free-run Characteristics

Figure 6 shows the slowdown of the speed during free-run operation. Careful observation allows us to recognize that an inflection point exists at about 15 Hz, and the rate of the speed decrease was higher at speeds less than 15 Hz. It can be assumed that the rotor contacted with the stator and the dry-friction decelerated the rotor speed. This assumption is clearly confirmed from Fig. 7 and Fig. 8. Figure 7 is the total mechanical loss calculated from Fig. 6. The mechanical loss of the rotor is equal to $-I_p\omega(d\omega/dt)$, where I_p is the polar moment of inertia, ω is the rotational angular velocity, and t is time.

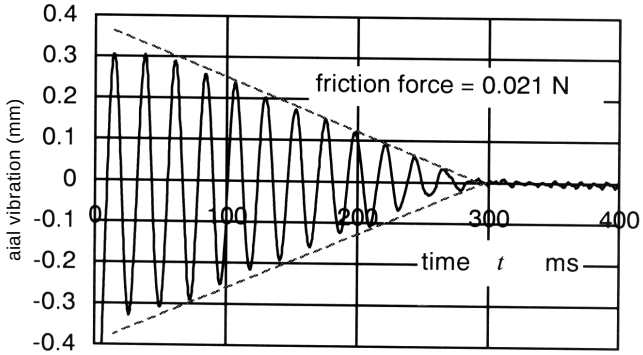

Figure 5. Axial free vibration at zero speed. ($2\pi\omega_n$ = 43.7 Hz, frictional force = 0.021 N)

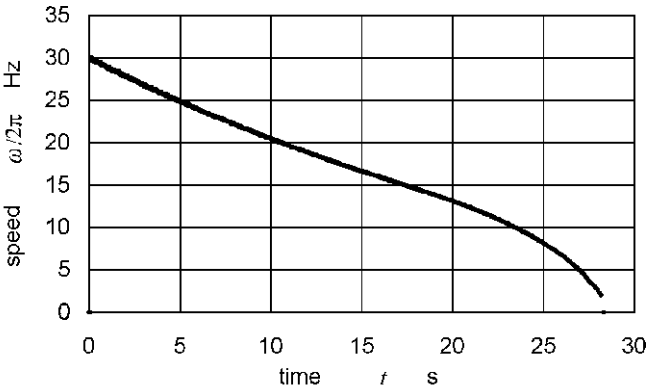

Figure 6. Slowdown of speed during free-run operation.

If the mechanical loss were solely due to the air drag, it would be proportional to the square of the speed. The measured loss actually coincided with the curve of secondary degree at the speed higher than 15 Hz but it is larger than the curve at less than 15 Hz, although the dispersion of the transformed loss data was substantially large due to the numerical differential $\Delta\omega/\Delta t$. The difference between the measured loss and the curve of secondary order may be caused by dry friction. Here, the curve was fitted by the least squares method using data at speeds higher than 16 Hz. Figure 8 shows the frictional force derived from the difference of the losses. The frictional force F is $(W_{total} - W_{airdrag})/(\omega r_0)$, where W_{total} is the total loss during free-run, $W_{airdrag}$ is the loss due to the air drag, and r_0 is the radius of the air bearing. The frictional force extrapolated at zero speed was about 0.03 N, which agreed fairly well with the force of 0.021 N derived from the free vibration curve at zero speed (Fig. 5). The two independently measured forces were consistent with each other, although the former is circumferential and the later is axial.

The evidence for dry friction during the startup operation could not observed directly because the rate of speed increase was extremely fast (68 Hz/s) in order to measure the small change in the torque. The radial abnormal whirling vibration due to dry friction[12,13] was also not observed, because the radial gap of the air bearing was only 5 μm and no substantial vibration took place in the radial direction.

Evaluation Indices

The following three indices were proposed to evaluate reliability against dry-contact. The durability is poor

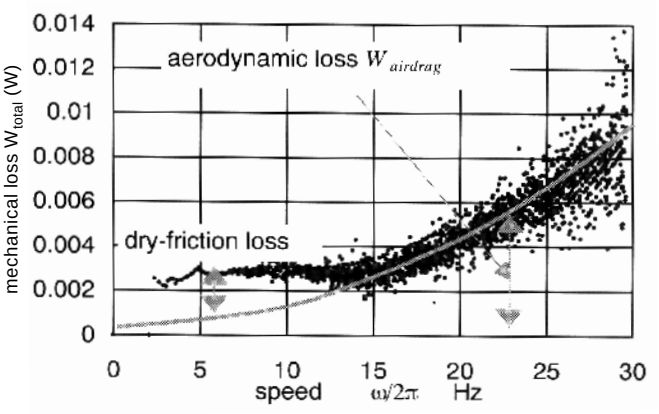

Figure 7. Mechanical loss during free-run operation.

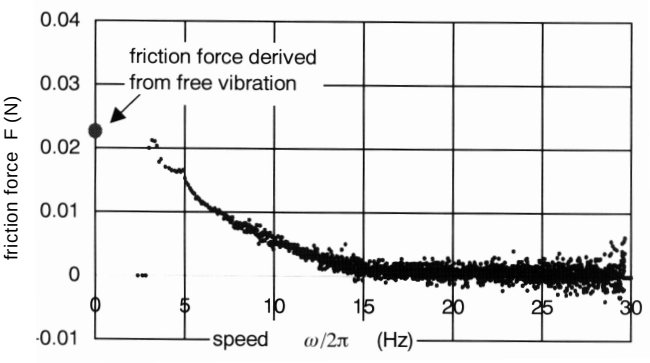

Figure 8. Dry-frictional force during free-run operation.

and the lifetime may be statistically short for a motor with high values of these indices.

(1) Critical contact-speed: One of the evaluation indices is the critical contact-speed. The rotor contacts with the bearing shaft (stator) at speeds lower than the critical speed, that is determined by the procedure described above.

(2) Frictional force: Because the frictional force is derived from the numerical differential of the free-run speed, it is impossible to derive the stationary frictional force. The frictional force at low speed, 5 Hz, just before stopping, is used in place of that at zero speed.

(3) Frictional energy: Frictional energy is the product of the frictional force F and the slip length $\omega r_0 t$. Because the frictional energy is a denominator of the specific wear rate in case of the friction coefficient $\mu = 0$, it is a relative index of the wear rate due to dry friction. Figure 9 shows the product of the contact load and the slip speed during free-run. Shaded area corresponds to the frictional energy.

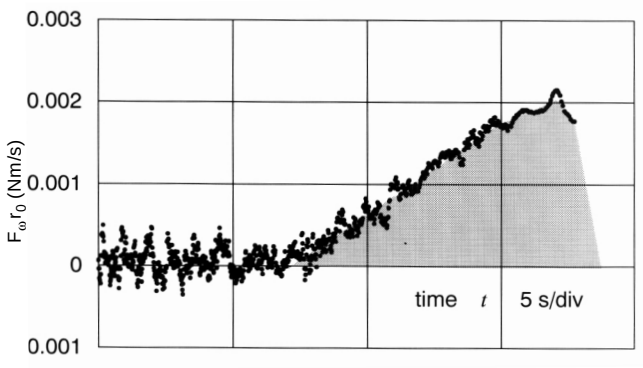

Figure 9. Product of contact load and slip speed during free-run.

Effect of Gravity

The effect of gravity was evaluated using three motors, motors 1, 2, and 3, in horizontal support and four directions of vertical support as shown in Fig. 4. The three indices we measured are summarized in Fig. 10. Each experiment was repeated three times under the same conditions. Averaged values are indicated in Fig. 10; three results coincided within 10% difference.

The rotor contacts with the stator when the static displacement due to the magnetic unbalance and the gravity plus the radial vibration of the rotor δ_u [15] is larger than the bearing gap Δ.

$$\Delta \le \frac{\left|\mathrm{F}_m + \mathrm{F}_g\right|}{k_a(\omega) - k_m} + \delta_u(\omega) \qquad (1)$$

The static displacement is determined by dividing an absolute value of the magnetic radial unbalance force $\boldsymbol{F}_m$ and the gravitational force $\boldsymbol{F}_g$ by radial effective stiffness. The effective stiffness is equal to the radial stable stiffness of the air bearing k_a minus the radial unstable stiffness of the magnetic bearing k_m. The magnetic unbalance force is caused by a radially non-uniform magnetization of the permanent magnets[10] and the gravitational force arises in the horizontal support. The mechanical unbalance of the rotor causes the radial vibration $\delta_u(\omega)$ which is a function of the speed.[14,15] The radial stable stiffness of the air bearing k_a is also a function of the rotor speed but other parameters, $\boldsymbol{F}_m$, $\boldsymbol{F}_g$, and k_m are almost constant with respect to the speed ω. The following are deduced from Fig. 10.

(1) The measured critical speeds were 5 – 20 Hz. Numerical calculation shown in Fig. 11 supported the experimental result. That is, the magnetic unstable stiffness is larger than the stiffness of the air bearing at speeds under 15 Hz, and therefore the static displacement, the first term on the right side of Eq. 1, becomes large when the rotor speed approaches 15 Hz. Here, aerodynamics of the grooved gas bearing was formulated based on the Reynolds equation derived from the mass conservation law in a bearing gap and the radial stiffness was numerically calculated by the perturbation and a Divergence Formulation-Finite Element Method.[16] On the other hand, the radial unstable stiffness of the magnetic bearing is indirectly estimated to be 6.7 N/mm, because the measured axial stable stiffness was 2.9 N/mm and the ratio of stable and unstable stiffness of the magnetic bearing composed of a pair of ring magnets is 0.43. A theoretical investigation deduced that the ratio is exactly one-half and it is independent of the geometry, if the permeability of the permanent magnet is equal to that of the free space. However, it is less than $2/\pi^2$ (= 0.2) and it varies with the geometry, if infinitely permeable material is used for pole yokes.[10] The measured ratio was about 0.43, a little smaller than 1/2, for several sizes of ring magnets made of ferrite magnet.

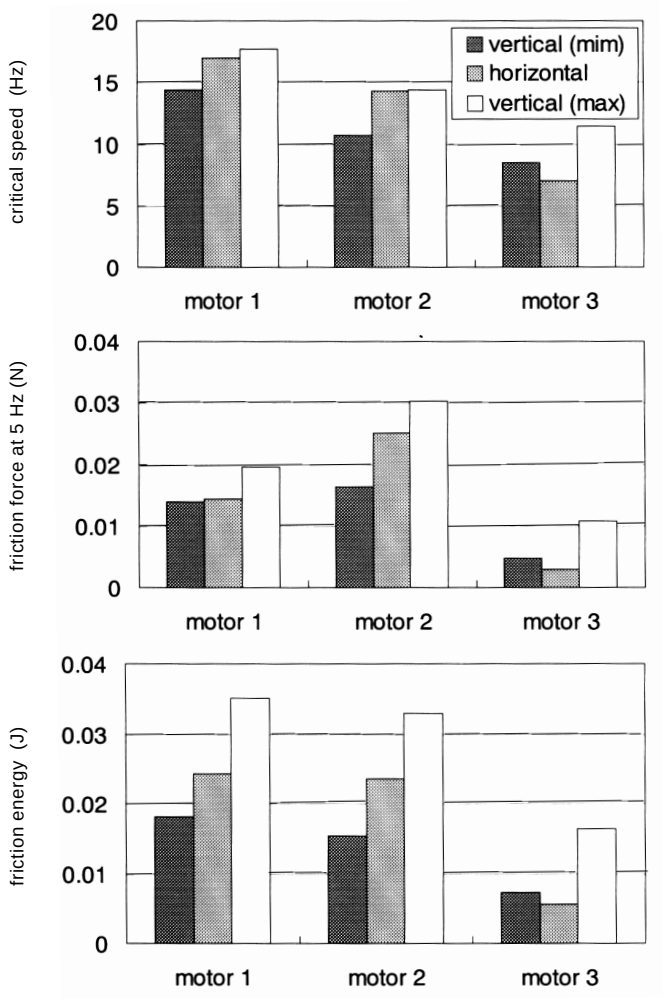

Figure 10. Measured indexes of reliability against dry friction.

This is probably because the relative permeability of the permanent magnet is not exactly 1.0 but about 1.1 - 1.2. Since this is also the case with our magnetic bearing, the ratio 0.43 is adopted to estimate the radial unstable stiffness from the axial stable stiffness of the magnetic bearing.

(2) The indices varied widely, about a factor of two, among the three motors. The reason for these differences is probably due to the dispersion of the air gap and the radial magnetic unbalance force, because the radial stiffness of the air bearing is greatly affected by the air gap. On the other hand, the measured dispersion of the stiffness of the magnetic bearing was less than 10 % and the effect of mechanical unbalance was small as cited in the following section.

(3) The vertical support led to about several tens percent change in the indices. This means that the magnitude of the gravitational force F_g is about several tens percent of that of the magnetic force F_m. Although the reliability of the vertically supported motor will be reduced about several tens percent compared to the horizontally supported motor, it seems to be tolerable for the present case, because it was confirmed that no trouble occurred in more than one hundred start-stop operations with the vertical support for three motors.

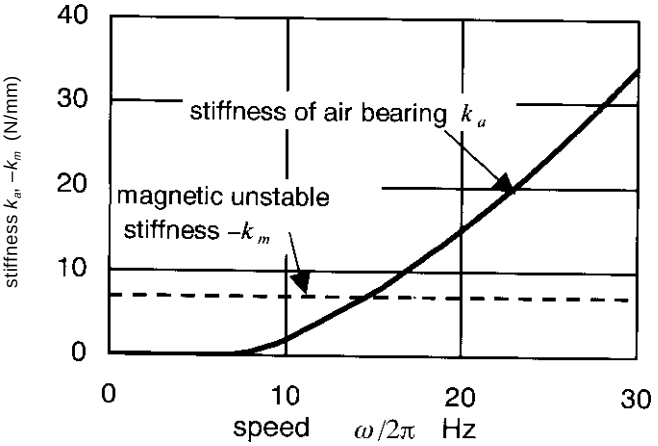

Figure 11. Stiffness of air bearing and magnetic unstable stiffness.

(4) Three indices correlate with each other. A motor with low critical speed, for example, is good with respect to both the frictional force and the frictional energy.

Effect of Rotor Unbalance

Effect of mechanical unbalance of the rotor was quantitatively investigated with an intentionally unbalanced rotor. Experiments were conducted in the horizontal support mode using motor 3 whose indices were smallest compared to other two motors. Figure 12 shows the three indices versus appended imbalance. Residual imbalance without intentional addition was less than 0.04 gm. It is clearly recognized that the effect of the rotor unbalance is negligibly small and the magnitude of the forced vibration, the second term on the right side of Eq. 1, is negligible compared to the static displacement, the first term on the right side of Eq. 1.

Discussion

The following methods are effective to improve reliability with respect to contact phenomena.

(1) The stiffness of the air bearing must be designed to be large, particularly in the low speed region. The numerical method, i.e., the Divergence Formulation-Finite Element Method,[16] is useful for rational design. We must determine design parameters of the air bearing, such as air gap, groove width, and groove depth, considering not only the stiffness but also dynamic stability[4–8] and cost issues.

(2) On the other hand, the radial unstable stiffness of the magnetic bearing must be designed to be as low as possible. This is inconsistent with realizing the high axial stiffness that is necessary to suppress the axial displacement and vibration under conditions of start–stop operation.[11] A magnetic bearing using a pair of permanent magnets is better than one using steel yokes, in order to minimize the unstable/stable stiffness ratio.[10]

(3) The static magnetic unbalance of the magnetic bearing must be minimized. Magnetically uniform magnets must be used and/or magnetic balancing must be carried out.[10] Magnetic balancing is a procedure to minimize the difference between the magnetic center and the bearing center.

(4) The idling speed must be set higher than the threshold, if the motor is not stopped but driven at low speed during idling periods.

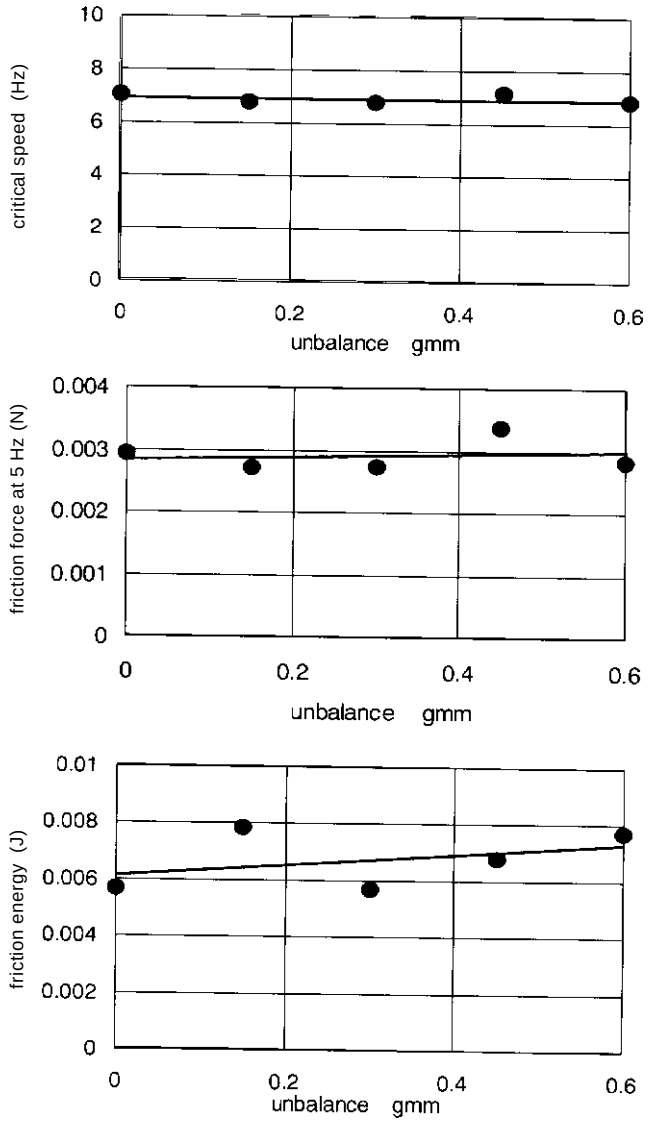

Figure 12. Measured reliability indexes of mechanically unbalanced rotor.

Concluding Remarks

Analytical and experimental investigations has been performed on the radial dry-contact in the low speed region of operation of a polygonal mirror scanner supported by a passive thrust magnetic bearing and radial air bearing. From results of these investigations, the mechanism and characteristics of dry contact have been clarified, and some countermeasures to improve reliability against dry-contact have been proposed. The present procedure and the proposed indices are useful to evaluate reliability of the motor.

Acknowledgment. The author would like to express his thanks to Mr. Ryosuke Okimura (Suzuka Fuji Xerox) for supplying the scanner motor and its design data. The numerical calculation on the stiffness of the air bearing was conducted using a program originally coded by Dr. Chao Chen and Prof. Nobuyoshi Kawabata (Fukui Univ.) and modified by Dr. Tomoyuki Ito (Fuji Xerox). The author also thanks Mr. Hirokazu Kurioka (Waseda University) for carrying out the experiment.

References

1. E. M. Williams, *The Physics and Technology of Xerographic Processes*, Krieger Publishing, Florida, 1993.
2. J. M. Fleischer, M. R. Latta and M. E. Rabedeau, *IBM J. Research and Development* **21**, 479 (1977).
3. S. P. Sarraf, Proc. *SPIE* Vol. **1079**, Hard Copy Output, 443 (1989).
4. J. H. Vohr and C. Y. Chow, *Trans. ASME D* **87**, 568 (1965).
5. K. Ono, A. Iwama, M. Suzuki, T. Iwamura, Y. Itami and T. Hwang, *J. Trans. of Japan Soc. of Mechanical Engineers C*, **60**, 2670 (1996).
6. T. Y. Hwang, K. Ono and Y. Itami, *Proc. of Int. Conf. on Micromechatronics for Information and Precision Equipment* (MIPE'97), The Japan Soc. of Mechanical Engineers, Tokyo, 1997, p. 607.
7. S. B. Malanoski, *Trans. ASME F* **89**, 433 (1967).
8. R. E. Cunningham, D. P. Fleming and W. J. Anderson, *Trans. ASME F* **91**, 52 (1969).
9. H. Kawamoto, *Bulletin of the Japan Soc. of Mechanical Engineers* **26**, 1654 (1983).
10. H. Kawamoto, Magnetic Bearing for High Speed Rotors, PhD thesis, Tokyo Institute of Technology, 1983.
11. H. Kawamoto, *J. Imaging Sci. Technol.* **43**, 484 (1999).
12. H. Kawamoto, *Nonlinear Dynamics*, **16**, 153 (1998).
13. A. Tondl, *Some Problems of Rotor Dynamics*, Czechoslovak Academy of Sciences, Prague, 1965.
14. H. Kawamoto, *J. Imaging Sci. Technol.* **41**, 565 (1997).
15. R. Gasch and H. Pfutzner, *Rotordynamik-eine Einfuhrung*, Springer-Verlag, Berlin, 1975.
16. C. Chen, N. Kawabata and M. Tachibana, *J. Trans. Japan Soc. of Mechanical Engineers C*, **63**, 2093 (1996).